Characterizing the evolution of mass flow properties and dynamics through analysis of seismic signals: Insights from the 18 March 2007 Mt. Ruapehu lake-breakout lahar

Braden Walsh[1], Charline Lormand[2], Jon Procter[3], Glyn Williams-Jones[1]

[1]Department of Earth Sciences, Simon Fraser University, Burnaby, British Columbia, Canada

[2]Department of Earth Sciences, University of Durham, Durham, DH1 3LE, UK

[3]Volcanic Risk Solutions, Institute of Agriculture and Environment, Massey University, Palmerston North, New Zealand

Corresponding Author: Braden Walsh (braden_walsh@sfu.ca)

Abstract

Monitoring for lahars on volcanoes can be challenging due to the ever-changing landscape which can drastically transform the properties and dynamics of the flow. These changes to the flows require the need for detection strategies and risk assessment that are tailored not only between different volcanoes, but at different distances along flow paths as well. Being able to understand how a flow event may transform in time and space along the channel is of utmost importance for hazard management. While visual observations and simple measuring devices in the past have shown how lahars transform along the flow path, these same features for the

most part have not been described using seismological methods. On 18 March 2007 Mt. Ruapehu produced the biggest lahar in New Zealand in over 100 years. At 23:18 UTC the tephra dam holding the Crater Lake water back collapsed causing $1.3x10^6$ m^3 of water to flow out and rush down the Whangaehu channel. We describe here the seismic signature of a lake-breakout lahar over the course of 85 km along the Whangaehu river system using three 3-component broadband seismometers installed <10 m from the channel at 7.4, 28, and 83 km from the crater lake source. Examination of 3-component seismic amplitudes, frequency content, and directionality combined with video imagery and sediment concentration data were used. The seismic data shows the evolution of the lahar as it transformed from a highly turbulent out-burst flood (high peak frequency throughout), to a fully bulked up multi-phase hyperconcentrated flow (varying frequency patterns depending on the lahar phase) to a slurry flow (bedload dominant). Estimated directionality ratios show the elongation of the lahar with distance down channel, where each recording station shows a similar pattern, but for differing lengths of time. Furthermore, using directionality ratios shows extraordinary promise for lahar monitoring and detection systems where streamflow is present in the channel.

Deleted: n

Deleted: peak

1. Introduction

Volcanic mass flows (e.g. debris flows, pyroclastic density currents, debris avalanches) are one of the greatest threats to communities, industry, recreation, etc. on and around volcanoes. These volcanic mass flows are particularly dangerous as they are fast moving turbulent flows that can occur without any warning or an eruption transpiring (Capra et al., 2010). These flows can move a sizable amount of liquid and debris great distances that can critically impact

locations hundreds of kilometers from the volcano or source. Lake-breakout or outburst flood events can be particularly destructive because they tend to be larger and can cause long lasting changes to the landscape and surrounding ecosystems (O'Connor et al., 2013; Procter et al., 2021). Furthermore, unlike eruption or rain triggered mass flows, outburst floods have very little to no warning. Eruption sources can be prepared for by the onset of the eruption and/or the monitoring of the volcano through various methods (e.g. seismology, infrasound, gravity, gas and water chemistry). Likewise, for rain-induced flows using techniques such as the amount or intensity of rain (e.g. Capra et al., 2010; 2018) or by monitoring the amount of available material (e.g. Iguchi, 2019) can help forecast when an event may occur.

In New Zealand, there have been numerous cases of large damaging mass flows in modern times. In October 2012, a lake-breakout lahar originating from Te Maari, destroyed hiking trails and forestry, eventually flowing over 4.5 km to damage and block off Highway 46 (Procter et al., 2014; Walsh et al., 2016). Moreover, on 24 December 1953, the deadliest lahar in New Zealand history occurred killing 151 people when a lahar struck a train crossing at the Tangiwai Rail Bridge, 39.8 km from the Crater Lake on top of Mt. Ruapehu (O'Shea, 1954). The ability to predict and investigate the changing dynamics and properties of large volcanic mass flows as they progress down channel is the first step in beginning to understand flow mechanisms better, and ultimately address the hazards involved to mitigate the risk.

In order to better characterize and understand these flow events, many applications and instruments have been used in the past (e.g. trip wires, stage gauge, load cells, pore pressure). While many of these tools can yield quick assessments and provide ample warning (e.g. current

meters, trip wires), they can sometimes be at risk of false detections, equipment damage or loss, and/or lack the capability to evaluate multiple pulses or flow events. Geophysical instruments (e.g. seismometers, geophones, infrasound) on the other hand can be installed at a safe distance away from the channel and have shown signs of not only being capable warning systems (e.g. Coviello et al., 2019), but have the ability to accurately estimate flow properties (e.g. Arattano and Marchi, 2005; Doyle et al., 2010; Schimmel et al., 2021), as well as flow dynamics (e.g. Gimbert et al., 2014; Coviello et al., 2018; Walsh et al., 2020). However, in order to fully utilize these instruments, improved interpretation, comprehension, assessment, and universality is needed. One technique to increase the ability to predict, warn, and estimate the properties and dynamics of flow events is to use all three components of the seismic recording. Recently, several studies have shown that using all three components is effective in characterizing flow events (e.g. snow-slurry lahars, Cole et al., 2009; snow avalanches, Kogelnig et al., 2011; streamflow, Roth et al., 2016; landslides, Surinach et al., 2005; lahars, Walsh et al., 2020; rockfalls, Kuehnert et al., 2021; hyperconcentrated flows, Walsh et al., 2016). Using the horizontal components along with the vertical component can yield additional information about the flow that is not utilized if only the vertical component is used. Notably, directionality analysis (e.g. Doyle et al., 2010; Walsh et al., 2020) can provide information about wetted perimeter, sediment concentration, and number of particle collisions. Furthermore, differing energies and frequency outputs from channel parallel and channel perpendicular signals can point to specific changes within the flow (Burtin et al., 2010; Roth et al., 2016) that can provide insights into the internal dynamics.

Deleted: the properties and dynamics of flow events

Deleted:

Deleted: To this extent, using geophysical instruments for mass flow monitoring is still relatively young and in need of more comprehension, assessment and universality.

Deleted: was previously not recorded

Formatted: English (US)

1.1 Anatomy of lahars

When a lahar is created from a lake-breakout or outburst flood event, the transition from flood or streamflow torrent depends on the erosivity of the channel and the supply of sediment being entrapped within the flow (e.g. Scott, 1988; Doyle et al., 2011). An event may start as a highly turbulent low sediment flow, then transform into a hyperconcentrated flow, and may even eventually 'bulk up' to exhibit characteristics of a debris flow with the possibility of laminar or plug-like behavior (Scott, 1988, Pierson et al., 1990). At Mt. Ruapehu, the propagational differences of lahars down channel have been observed and characterized in the past (e.g. Cronin et al., 1996; Cronin et al., 1999; Cronin et al., 2000; Manville et al., 2000; Procter et al., 2010a; Lube et al., 2012). From these studies, models of how lahars bulk up and transition throughout the run-out distance have been postulated. For the lahars in the Whangaehu channel, Cronin et al. (1999) created three 4-phase conceptual models based on source distances of 23.5 km, 42 km, and >55 km. The first two models are for lahar regimes, whereas the third model described a lahar almost at its peak run-out distance. In each model, the first phase consists of a super charged streamflow pulse that flows ahead of the head of the flow. This phenomenon has also been noted for debris flows interacting with streamflow (Arattano and Moia, 1999). Furthermore, discharge is maximum at the transition between phase 1 and phase 2 (Cronin et al., 1999). Phase 2 is described as a mixing zone between streamflow and increasing sediment content, where the peak sediment concentration usually occurs at the end of phase 2 or at the beginning of phase 3 (e.g. Pierson and Scott, 1985). Cronin et al. (1999) defined phase 3 as the lahar body, which has the least amount of the original streamflow contained within. Phase 3 is also characterized by coarse sediment suspensions and is the most likely location for debris flow rheology. Finally, phase 4 is the tail of the lahar where debulking

and dilution occurs transforming the lahar back into a hyperconcentrated, mixed, or streamflow.

1.2 18 March 2007 lake-breakout event

Mt. Ruapehu (2797 asl) is the largest stratovolcano in the central North Island of New Zealand (Figure 1) which sits at the southwestern end of the Taupō Volcanic Zone (TVZ). The volcano has a volume of 110 km^3 which is composed of several overlapping cone building formations and surrounding ring plain volcaniclastics (Carrivick et al., 2009; Pardo et al., 2012). On top of the volcano, above the currently active vent sits a $1x10^7$ m^3 acidic crater lake (Procter et al., 2010a). The Whangaehu channel is the preferred outlet for Crater Lake water and lahars in recent history (Procter et al., 2012; Procter et al., 2021). The Whangaehu channel is on the eastern flank of Mt. Ruapehu where it runs down across the volcanic ring plane where it eventually heads southwest for ~200 km reaching the Tasman Sea.

Prior to the events that took place in the morning local time on 18 March 2007, a heavy rainstorm occurred accumulating about 256 mm of water over the 10 hours prior to the dam breach that led to the outburst flood (Massey et al., 2010). The intense rain caused the Crater Lake to rise an extra 6.4 m above the natural lava formation ledge, which started to cause seepage and extra water entering the Whangaehu gorge (Carrivick et al., 2009). At ~11:18 NZT (UTC +12), the tephra dam collapsed causing $1.3x10^6$ m^3 of water to flow out of the lake and into the Whangaehu channel (Procter et al., 2010a). The dam was eroded and undercut in multiple stages resulting in a series of retrogressing landslides along with the main debris flow/lahar channel.

Deleted: River

Deleted: River

Deleted: GMT

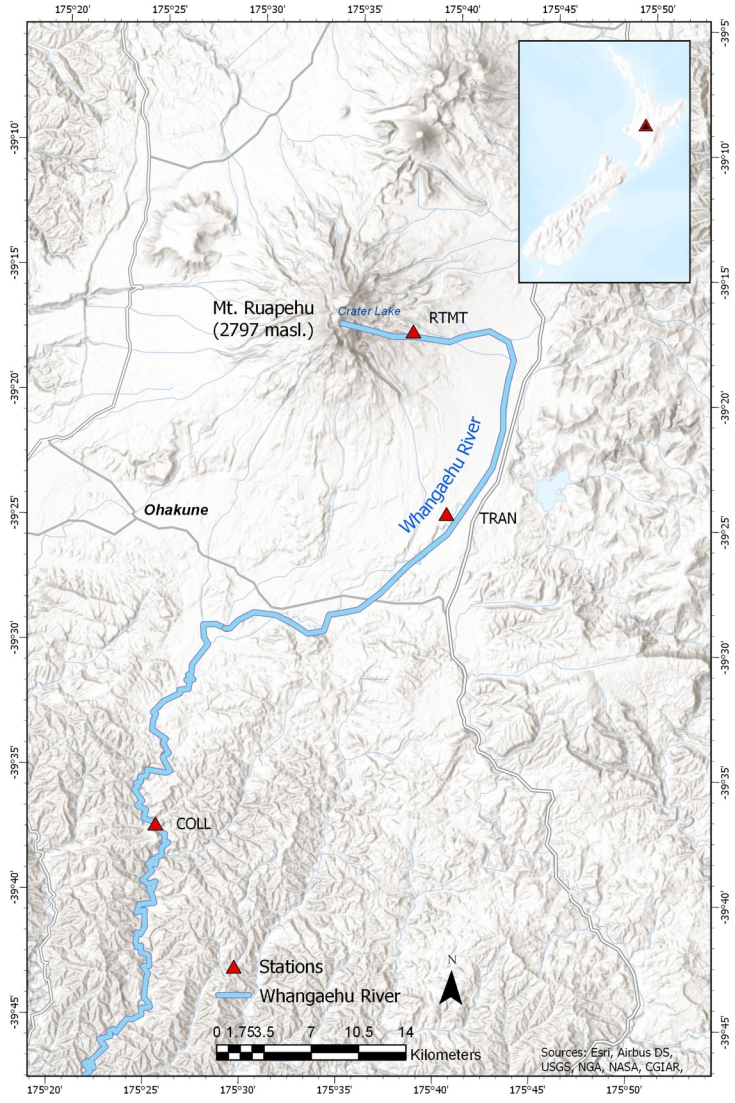

138

139 *Figure 1 Map of Mt. Ruapehu and the surrounding area located on the central North Island of New Zealand. Blue*
140 *outline represents the Whangaehu channel and the path the 18 March 2007 lahar traveled down. Red triangles*
141 *denotes the three monitoring stations along the Whangaehu channel at 7.4, 28, and 83 km.*

Since the lahar was caused by lake-breakout dynamics and thus an abundance of water, the event was classified as a hyperconcentrated streamflow rather than a sediment-filled debris flow (Procter et al., 2010b). At ~8.0 km from source velocity measurements recorded the flow at ~ 9.5 m/s and had an estimated 6 m of downcutting showing the ability for the lahar to deposit and erode massive amounts of material (Procter et al., 2010a,b). Furthermore, the 18 March 2007 lahar was one of the most thoroughly monitored lahars ever (Manville and Cronin 2007). In total there were 21 monitoring locations setup to measure various lahar properties, (e.g. flow monitor, camera, stage height, flow sampling, pore-pressure, seismic, etc.) along the channel (Keys and Green, 2008; Lube et al., 2012), with the lahar taking over 16 hours to eventually travel out to the New Zealand coast, ~200 km from the original crater lake source.

Here, we delve into the properties of a lake-breakout hyperconcentrated streamflow that bulked up to a volume of ~4.4×10^6 m^3 (Procter et al.,2010a) over the course of 83 km that occurred on 18 March 2007 along the Whangaehu channel originating from Mt. Ruapehu, New Zealand. The combination of seismic analysis (frequency and directionality) with supplementary measurements (e.g. video, sediment concentration) show how a lahar transforms over time and distance and how using these seismic techniques can help monitor the ever changing dynamics and properties of a flow event. Furthermore, we examine previous models of the evolution of a lahar and compare the model with the seismic data available.

Deleted: River

Deleted: on-the-ground

2. Data

The seismic data for the 18 March 2007 lahar was recorded on three seismometers installed at various distances (7.4, 28, 83 km) along the Whangaehu channel (Figure 1). The three 3-

component broadband Guralp 6T sensors (COLL, RTMT, TRAN) recorded data at 100 Hz sampling and had GPS time stamps. For each site, the seismometers axes were installed to true North and the recorded data were rotated to align North as flow parallel (P) and East as the cross-channel direction (T). Furthermore, the seismometers were installed normal to horizontal to lessen the degree of vertical energy transfer to the horizontal components. The monitoring station Round the Mountain Track (RTMT), was installed 4 m from the channel and 7.4 km downstream from the source of the lahar. The lahar arrived at RTMT at 23:36 UTC and had an average velocity of 9.3 m/s (Figure 2a). The Trans Rail Gauge (TRAN) station was installed 28 km from source and 10 m from the channel, which also included a video camera that captured an image every 30 seconds. The lahar arrived at TRAN at 24:35 UTC with an average velocity of 5.6 m/s (Figure 2d). The Colliers Bridge (COLL) station was installed 10 m from the channel and 83 km from source. The lahar arrived at COLL at 04:13 UTC and had an average velocity of 4.8 m/s (Figure 2f). Arrival times are based off of images and eye witnesses at each of the monitoring stations. The flow velocity at RTMT and COLL were estimated from imagery and at TRAN from a flow meter.

Deleted: 11

Deleted: 12

Deleted: 16

3. Results

To examine the multi-component dynamics of the 18 March lake-breakout event along the Whangaehu channel at three monitoring locations, the data were corrected for instrument response and split into 10 s time windows. At each recording location, peak spectral frequency (PSF) amplitude, root mean squared (RMS) amplitude, and directionality ratios (DR) are estimated for each of the 10 s time windows. At each monitoring station the first hour of the

lahar including five minutes prior to the arrival are shown in all the results except when indicated.

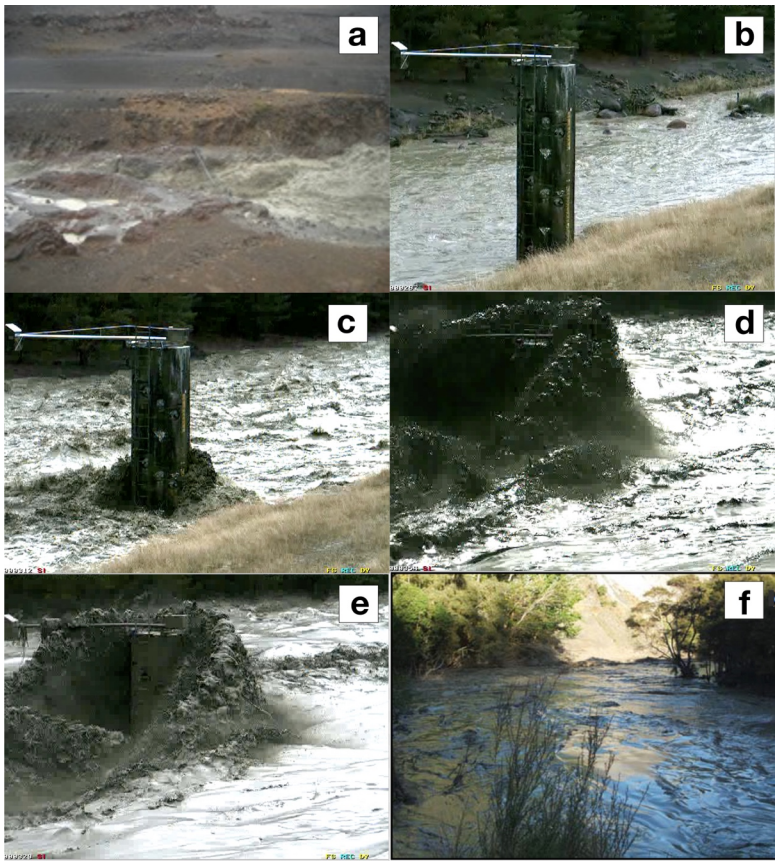

Figure 2 Images from the 18 March 2007 lake break-out lahar from RTMT (a), TRAN (b, c, d, e), and COLL (f). Note the transformation of the lahar at TRAN from streamflow (b), increased discharge pre-lahar phase 1 pulse (bow wave) (c), head of the lahar (d), and low PSF beginning of lahar body (e).

3.1 Frequency analysis

In order to examine the PSFs for all three components at each site along the channel, we use the frequency recorded at the maximum amplitude of the frequency spectra for each 10 s running time window. The PSF for RTMT (7.4 km from source) shows similar patterns between all three components (Figure 3). The five minutes prior to the arrival of the head (peak seismic amplitude) of the lahar are characterized by scattered PSFs between 20-40 Hz for the cross-channel (Figure 3, blue dots) and parallel (Figure 2, red dots) directions, while in the vertical direction (Figure 3, green dots) the PSF is ~30 Hz. When the front of the lahar arrives at the station, the PSF in all three components decreases to ~5-10 Hz for about 1 min before increasing again to higher frequencies. After the front of the lahar passes the station and when the head arrives the PSF in the cross-channel and parallel directions remain between 30-40 Hz for the rest of the recording window. In the vertical component, the PSF is scattered between 20-40 Hz for ~15 min after the arrival of the head of the lahar and then becomes narrower, similar to both the cross-channel and parallel components with PSFs between 30-40 Hz.

Deleted: F

Deleted: (streamflow)

Deleted: are

Deleted: (peak seismic amplitude)

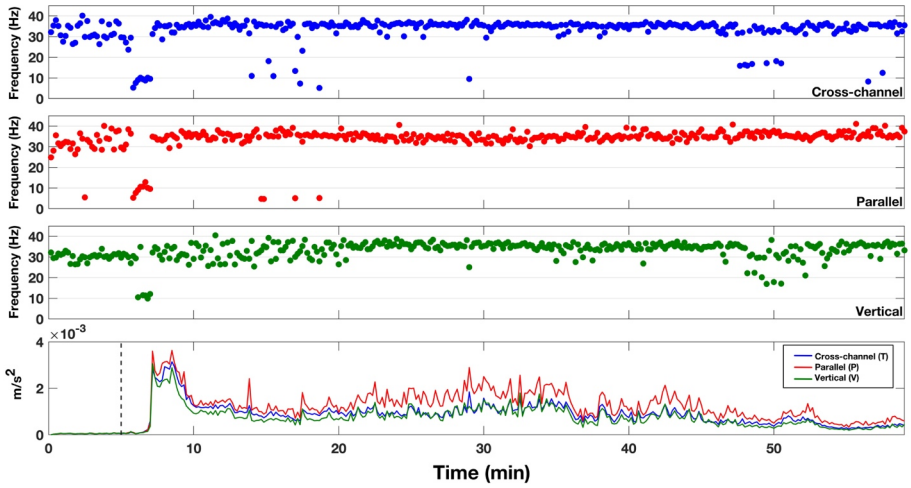

Figure 3 Peak spectral frequencies for RTMT (7.4 km from source) for cross-channel (blue dots), flow parallel (red dots), and vertical (green dots) directions. Bottom row depicts the RMS amplitude of the lahar color coded to the same colors as the PSF. The dashed vertical line marks the timing of the lahar front passing the monitoring station. All PSFs and RMS amplitudes were calculated using 10 s time windows.

Deleted: *r*

Deleted: *passing the station*

Further down the channel at station TRAN (28 km from source), the PSFs for all three components show a similar overall pattern (Figure 4). The pre-lahar PSF distribution in all three components is between 20-32 Hz. Like RTMT higher up the channel, the PSFs for the front of the lahar at TRAN first drops down to around 10 Hz and when the lahar head arrives (10 min, Figure 4) the PSF increases to ~30 Hz for parallel (Figure 4, red dots) and cross-channel (Figure 4, blue dots) directions and between 20-30 Hz in the vertical component. This decrease to lower frequencies before the head of the lahar at TRAN lasts for about 5 min. After the head of the lahar passes the recording station the PSF content decreases for ~15 min to 10-20 Hz for the parallel and cross-channel components and between 10-25 Hz for the vertical (Figure 4, green dots) components. The PSF after the 30 minute mark in Figure 4 displays a bimodal

pattern with frequencies between 10-35 Hz, with PSF time windows concentrating most at ~30 Hz.

At the COLL recording station (83 km from source), the PSF distribution shows differing patterns for all three components (Figure 5). The PSF in the cross-channel direction (Figure 5, blue dots) depicts a bimodal pattern throughout with a strong lower concentration of time windows at ~18 Hz and a higher PSF at ~25 Hz. For the parallel component (Figure 5, red dots), the pre-lahar signal has a wide PSF range between 12-30 Hz. When the lahar arrives, the PSF becomes concentrated at ~22 Hz for ~8 min before transforming into a bimodal pattern similar to that of the cross-channel PSF, with frequencies between 20-30 Hz. In the vertical component (Figure 5, green dots), the PSF remains concentrated around ~28 Hz, only varying just prior to the arrival of the lahar and during the highest energy stage of the lahar (25-40 min).

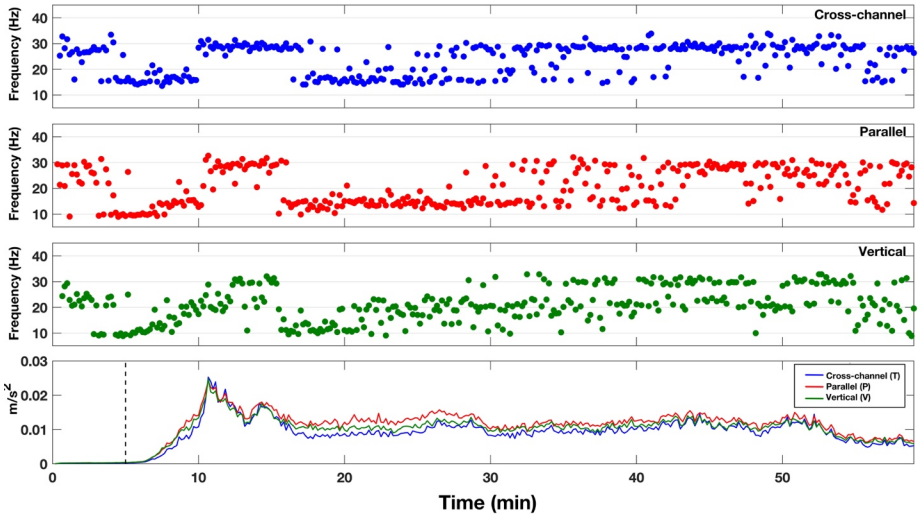

Figure 4 Peak spectral frequencies for TRAN (28 km from source) for cross-channel (blue dots), flow parallel (red dots), and vertical (green dots) directions. Bottom row depicts the RMS amplitude of the lahar color coded to the same colors as the PSF. The dashed vertical line marks the timing of the lahar front passing the monitoring station. All PSFs and RMS amplitudes were calculated using 10 s time windows.

Deleted: *passing the station*

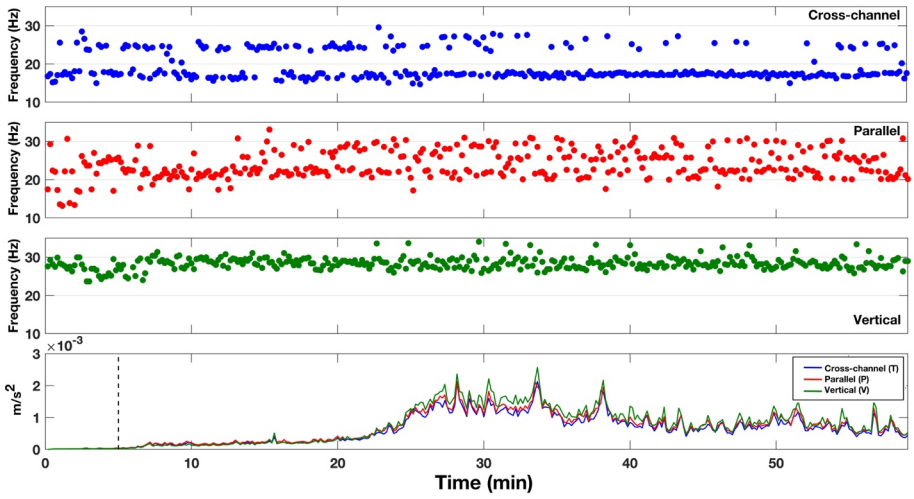

Figure 5 Peak spectral frequencies for COLL (83 km from source) for cross-channel (blue dots), flow parallel (red dots), and vertical (green dots) directions. Bottom row depicts the RMS amplitude of the lahar color coded to the same colors as the PSF. The dashed vertical line marks the timing of the lahar front passing the monitoring station. All PSFs and RMS amplitudes were calculated using 10 s time windows.

Deleted: *passing the station*

3.2 Directionality

When recording mass flows with 3-component sensors, the directionality may be examined due to the sensor being able to record signals in the two horizontal directions. The directionality ratio allows for the determination of which horizontal component has stronger energy over the course of the recording window. This is possible because, in channel side deployments for mass flow monitoring systems, the sensor is either installed so that the North component is aligned to be parallel to the flow or can be rotated during the data processing stage to align with the channel orientation. Furthermore, with the channel side installations, attenuational factors can mostly be ignored due to the close proximity to the channel and energy output of the flow event. The directionality ratio (DR) can be defined as the cross-channel amplitude divided by

Deleted: the

Deleted: aligned to North as flow parallel

Deleted: energy

the flow parallel amplitude. A DR > 1 indicates that the cross-channel amplitude is larger than that of the flow parallel, and vice-versa for a DR < 1. Directionality ratios have been used in the past to show rheology changes within flows for warning purposes, where the DR increases when streamflow transitions into a lahar (Walsh et al., 2020), and have been hypothesized to be an indicator for flow properties such as sediment concentration, wetted perimeter, and/or amount of particle collisions within a lahar (Doyle et al., 2010).

The directionality ratios for 10 s running time windows at each seismic station for the 18 March 2007 lake-breakout lahar are shown in Figure 6. The DR for RTMT (Figure 6a) displays a DR around 1 pre-lahar, then decreases right before the lahar arrives at the recording station (Figure 6, dashed line), then as soon as the lahar passes, the DR increases to above DR = 1 for ~2 min. After the initial lahar flood pulse passes RTMT, the DR then proceeds to decrease below a DR = 1 for the rest of the recording window. Similar to RTMT, the DR for TRAN starts out with a DR < 1 (0.7-0.8) and as the lahar front passes, the DR similarly decreases to 0.6-0.7 before increasing to a DR > 1 for ~5 min when the lahar is at peak energy output starting at about the 10 min mark (Figure 6d, red line). After the passing of the peak energy, the DR for TRAN decreases below 1 again for the remainder of the recording window. Further down the channel at COLL (Figure 6c), the DR before the lahar arrives has a wide range of values between 0.8-1.2. When the front of the lahar passes (Figure 6, dashed line), the DR stabilizes between 0.8-1, before increasing slightly when the peak energy of the lahar passes the monitoring site at about the 25 min mark.

Deleted: energy

Deleted: energy

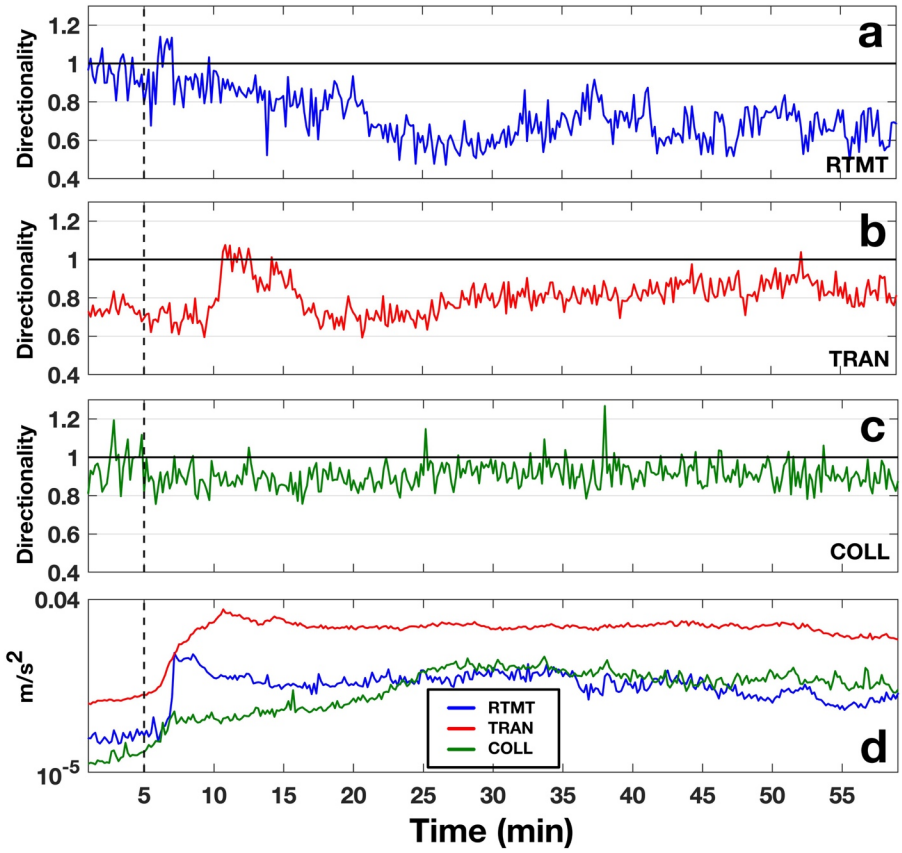

Figure 6 Directionality ratio plots over time for RTMT (a), TRAN (b), and COLL (c). Vertical RMS seismic signals for the three stations are plotted in (d) where blue is RTMT, red is TRAN and green represents COLL. The dashed vertical lines mark the timing of the lahar front passing the monitoring station. All DRs and RMS amplitudes were calculated using 10 s time windows.

4. Discussion

4.1 Frequency constraints

In order to obtain an understanding if PSFs are able to properly describe the lahar dynamics (i.e. the weight of the spectral amplitude at the PSF), frequency constraints must be analyzed. To complete this, normalized spectrograms along with spectral centroidal frequency (SCF) and spectral spreads are computed. The normalized spectrograms are estimated by normalizing the spectral amplitude for each 10 second time window of the lahar individually. By normalizing each time window, ranges of dominant frequencies can be visualized. SCFs are used because they represent the weighted average of the spectra, and yield the location (i.e. frequency) of the center of the spectral mass. The SCF of each time window is estimated similar to that of Saló et al. (2018), in which:

$$SCF = \frac{\sum_{f1}^{f2} f * A(f)}{\sum_{f1}^{f2} A(f)} \quad (1)$$

where *f* is the frequency and *A(f)* is the spectral amplitude associated with each frequency bin. The spectral spread measures the width of the spectral energy around the SCF, thus yielding information about the quality of the PSFs. Spectral spread can be estimated by:

$$S = \sqrt{\frac{\sum_{f1}^{f2} (f - SCF)^2 * A(f)}{\sum_{f1}^{f2} A(f)}} \quad (2)$$

The computed normalized spectrograms along with SCFs and spectral spreads for each of the three monitoring stations are shown in Figure 7. For simplicity and comparison, only the flow parallel data are shown. The normalized spectrograms for every station and component can be seen in Figures S1-S3.

The normalized spectrogram for RTMT (Figure 7a) yields very similar results to that of the PSF (Figure 3b), where most of the higher spectral amplitudes are at the same frequencies as those of the PSF. Notably, the low ~10 Hz signal immediately before the arrival of the head of the lahar is not only seen in the dominate normalized spectra, but also through the decrease in SCF. Additionally, the PSFs at these time windows are contained within the spectral spread (Figure 7a, black lines). For TRAN, the normalized spectrogram (Figure 7b) is again, very similar to the PSF in Figure 4b. The SCF mirrors the pattern of the PSF with higher frequencies for the streamflow, a decrease for the front of the lahar, increase for the head of the lahar, decrease after the passing of the head, and finally a slight increase later in the lahar body. The normalized spectra yields this same pattern, with the late lahar body displaying the only timeframe with increased spectral amplitude distributed throughout the spectral spread (Figure 7b, after 30 min). This most likely explains the bimodal distribution of PSFs for TRAN in Figure 4 after the ~30 min mark. Continuing, the normalized spectrogram for COLL (Figure 7c), also shows similarities to that of the PSFs in Figure 5b. The PSFs for COLL range between ~20-30 Hz with a slight bimodal pattern. This same pattern can be seen where the higher spectral amplitudes are located (Figure 7c). Furthermore, the SCF for COLL splits the PSF range and stays at ~25 Hz during the bimodal phase of the PSF. Overall, with the analysis of the normalized spectrograms, SCFs and spectral spreads, we confirm that the use of PSFs to describe mass flow dynamics is concise for the 18 March 2007 lake-breakout lahar.

Formatted: Font: Not Bold

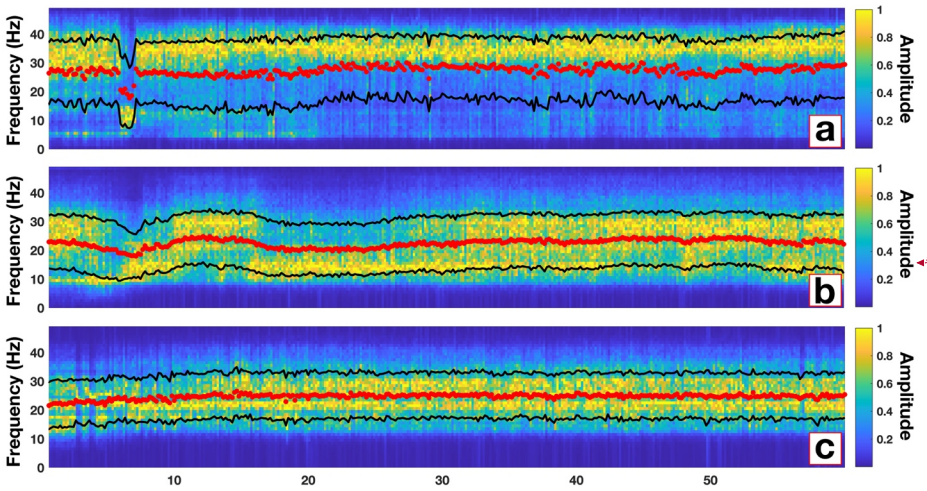

Figure 7 Normalized spectrograms for the flow parallel direction for each of the three monitoring sites along the Whangaehu channel. Red dots represent the spectral centroidal frequency and black lines show the range of the spectral spread. Note, normalized spectrograms for the other directions can be seen in Figures S1-S3.

4.2 Evolution of lahar signals

A lahar propagating down channel can bulk up by collecting material from erosion or through the coalescing of multiple pulses to shorten the total length of the lahar (Procter et al., 2010; Doyle et al., 2011). Lahars can also debulk by depositional means or by the natural elongation of the lahar as it progresses down channel (Doyle et al., 2011; Lube et al., 2012). Considering the 18 March 2007 lake-breakout lahar was a large pulse of water that only mixed with the existing streamflow and contained no juvenile material, examining the seismic signatures along the flow path can be used to characterize the evolution and transformation of a lake-breakout event from outburst flood to hyperconcentrated flow and beyond. At RTMT (Figure 3), the seismic signature is dominated by the flow parallel direction with > 30 Hz PSF. The exception to

Formatted: Keep with next

Formatted: Font: 10 pt, Font color: Text 1

Formatted: Caption, Space After: 0 pt, Line spacing: single

Deleted: 1

Deleted: combination

this is the timeframe immediately before the head of the lahar passes when the PSF decreases to ~10 Hz. This low frequency signal can be seen at TRAN (Figure 4) and in the flow parallel component at COLL (Figure 5, red dots). However, at COLL the PSF is ~20 Hz instead of 10 Hz as in RTMT and TRAN due to flow properties at 83 km from source. This low PSF before the head of the lahar arrives at the station could represent the supercharged stream flow pulse (bow wave) that is pushed in front of the head of the lahar as described by Cronin et al. (1999) where they noticed these same pulses in front of lahar heads for three lahars on Mt. Ruapehu in 1995. Conversely, this frontal pulse could be from the uplift of streamflow from the faster moving underflow of the lahar (Manville et al., 2000). Furthermore, the low frequency zone before the head of the flow lengthens as the lahar progresses downstream, suggesting that lahar elongation can also be seen in the seismic frequency domain. The ~10 Hz PSF may be explained by flow processes (Schmandt et al., 2013; Barriere et al., 2015; Bartholomaus et al., 2015) and could be due to the flow at this stage being more sensitive to discharge (Gimbert et al., 2014; Schmandt et al., 2017; Anthony, et al., 2018) or in the case of the underflow hypothesis, frictional sliding on the channel bed (Huang et al., 2004). The frontal surge or phase 1 of the lahar can be seen in the DR (Figure 6) as well. For every station along the channel the DR has a slight drop when phase 1 passes the recording station (Figure 6, dashed line). The elongation of phase 1 can also be seen, where the dip in the DR is only ~1 min for RTMT, ~5 min for TRAN, and approximately 20 min for COLL. The reason the DR decreases during phase 1 for the 2007 lahar could be due to the parallel component being more sensitive to flow processes than bedload forces (Barriere et al., 2015; Roth et al., 2016). During phase 1 discharge increases, sediment concentration is low, and streamflow dominates resulting in a low DR (e.g. Doyle et

al., 2010). The low DR can also be seen before the arrival of phase 1, due to streamflow already occurring in the channel. The higher flow parallel amplitude over cross-channel amplitude for streamflow has also been noted in the past for lahars at Volcán de Colima, Mexico (Walsh et al., 2020).

Following the low PSF phase 1 (i.e. front of the lahar), the peak seismic amplitude occurs. The peak seismic amplitude for RTMT is accompanied by an increase to higher PSFs > 30 Hz (Figure 3, 7a). PSFs > 30 Hz have been shown in the past to be either dominated by turbulence or bedload transport (e.g. Gimbert et al., 2014; Roth et al., 2016). The 2007 lake-breakout lahar has been described as a hyperconcentrated streamflow (e.g. Procter et al., 2010b) with low sediment concentration, especially early on before the lake water captured enough material to bulk up into a full 4-phase lahar (see section 1.1). At RTMT, which was only 7.4 km from source, the lahar had not fully bulked up yet and was in a net depositional regime (Procter et al., 2010a). Due to the conditions of the lahar at RTMT, we surmise the higher PSF content for the peak seismic amplitude is dominated by turbulent-flow-induced noise. Furthermore, the higher PSF content at RTMT compared to TRAN and COLL (~30 Hz) could be due to the angle of the slope at the recording stations. Gimbert et al. (2014) noted that turbulence noise will dominate over bedload-induced noise on steeper slopes. Further down the channel at TRAN, the PSF for the peak seismic amplitude is ~30 Hz for all three components. Again, this high PSF can be attributed to turbulence as seen by the images taken at TRAN (Figure 2d). The difference at TRAN is the length of the higher PSF, where at RTMT the high PSF stays throughout the entirety of the recording window, at TRAN the high PSF and seismic amplitude only last for ~5 min. The difference at TRAN could be from the evolution of the lahar. By time the lahar reached the

Deleted: energy

Deleted: energy

399 monitoring station at TRAN (28 km from source) the lahar was fully bulked up and had the
400 properties of a traditional four phase lahar as described by Scott (1988) or Cronin et al. (1999).
401 By time the lahar reached COLL 82 km from source, the peak seismic amplitude is associated
402 with PSFs between 15-30 Hz, with bimodal patterns in the horizontal components and a tighter
403 spread in the vertical component (~27-29 Hz). At COLL, the lahar had converted into a plug-like
404 flow with lower turbulence and hence the higher PSFs are most likely associated with bedload
405 transport (Figure 2f). Furthermore, Burtin et al. (2010) and Roth et al. (2016) noted that when
406 the vertical component has greater seismic amplitudes than the horizontal components,
407 bedload dominates. This same amplitude feature can be seen at COLL (Figure 5, bottom panel)
408 where the vertical energy is greater than each of the horizontal components. The bimodal
409 pattern of the horizontal components is likely to be the recording of both turbulence or flow
410 properties (lower PSF) and bedload transport (higher PSF). This also explains why the vertical
411 component does not show the same bimodal pattern. Barriere et al. (2015) described the
412 parallel component as being more sensitive to flow properties, and Doyle et al. (2010) noted
413 that the cross-channel component is likely dominated by turbulence, thus the reasoning behind
414 the differing PSF patterns between components. This PSF feature is similar to the lahars
415 recorded by Walsh et al. (2020), where the cross-channel PSF is confined within a narrow band
416 around 15-20 Hz and the flow parallel PSF is more bimodal. At COLL, the cross-channel PSF is
417 dominated by PSFs at ~18 Hz (lower than vertical component at ~28 Hz), with the flow parallel
418 between 20-30 Hz.

419 The DR at the peak seismic amplitude for all three recording stations increases (Figure 6). The
420 DR for both RTMT and TRAN increases to DR > 1. Doyle et al. (2010) noted that higher wetted

perimeters will increase the DR, which is true for the 18 March 2007 lake-breakout lahar (Figure 6, peak DR/RMS amplitude). Conversely, the DR decreases after the peak seismic amplitude while the wetted perimeter is still high. Also, at COLL the DR only increases slightly with the seismic amplitude. While the wetted perimeter may be a factor in increasing cross-channel energy and thus the DR, the more likely explanation for the 18 March 2007 lahar might be the higher level of particle collisions at the peak seismic amplitude. More particle collisions would increase the DR (e.g. Doyle et al., 2010) due to more lateral excitation within the flow and against the channel walls. The increase in collisional energy also relates well with the PSF, as higher PSF correlates to an increase in the amount of interflow collisions as shown by Huang et al. (2004) and may also explain why DRs correlate well with PSF (Figure 8a). The DR for COLL during this same timeframe probably is not due to the amount of particle collisions due to the plug-like flow (Figure 2f), but rather the increase in sediment concentration (Figure 8c). As the sediment concentration increases at COLL the DR starts to increase as well (Figure 8b). Similar to Doyle et al. (2010), COLL yields a correlation between DR and sediment concentration (Figure 8b), where higher DRs indicate higher concentrations of sediment contained in the flow. Lastly, as noted above, DRs may correlate with PSF or at least indicate differing processes taking place within the flow (Figure 8a). Lower PSF would produce lower DRs because low PSF are more sensitive to flow processes (hence higher parallel energy) whereas higher PSFs would produce higher DRs due to higher PSF being dominated by collisions and turbulence (higher cross-channel energy) (Figure 8a).

Deleted: 7

Deleted: 7

Deleted: 7

Deleted: 7

Deleted: 7

Deleted: 7

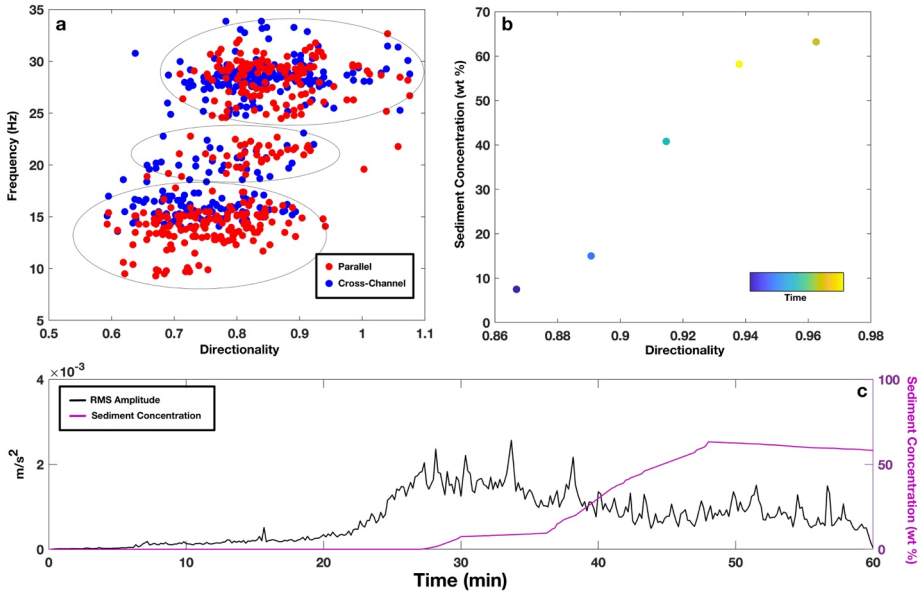

Figure 8 Plots of (a) correlation between PSF and DR at TRAN, (b) sediment concentration and DR at COLL, and (c) seismic amplitude (black line) with sediment concentration (purple line) depicting the lag in sediment at COLL. Note on (a) parallel (red dots) and cross-channel (blue dots) PSF display three different zones (black circles). Also note that at COLL the first sediment concentration measurement did not occur until the 30 min mark.

Deleted: 7

While the lahar at RTMT was a large outburst flood/sediment-laden flow, and at COLL a plug-like flow, at TRAN the 18 March 2007 lahar was a dynamic bulked up "traditional" lahar. The evidence for this is in the PSF content for TRAN (Figure 4) compared to the other two monitoring sites. At TRAN the PSF has a step-up step-down pattern for the first 30 min of the lahar passing, and then transitions to a bimodal or wide PSF range for the rest of the recording window. As noted above, the low PSF preceding the lahar head arrival is thought to be due to a sensitivity to water transport properties (Figure 2c). The increase to higher PSFs during the peak seismic amplitude may be from particle collisions and/or higher turbulence (Figure 2d). After the maximum seismic amplitude at TRAN, the PSF decreases to 10-20 Hz. This drop in PSF after

462 the highest stage and amplitude could be from a more water transport dominated regime,
463 which can be seen in the increased parallel amplitude (Figure 4, 8a). The decrease may also be
464 from greater frictional sliding on the channel bed (Huang et al., 2004). Furthermore, this PSF
465 range could simply indicate a decrease in turbulence (Figure 2e). After the decrease to 10-20 Hz
466 PSFs, the PSF displays a bimodal or wide frequency range at ~28 min (Figure 4, 7b). As
467 aforementioned for COLL, this PSF pattern could be from both bedload- and water-transport-
468 induced noise. This timeframe is also where the peak sediment concentration would be, as
469 noted by Cronin et al. (1999), and thus the PSF would show more bedload high PSF. This
470 hypothesis also compares well with the DR (Figure 6b), where the cross-channel energy
471 increases starting at ~25 min indicating that the sediment concentration may be increasing
472 (Doyle et al., 2010). Finally, the wide PSF range later in the recording window (Figure 4) could
473 also result from the lahar having two distinct layers as described by Cronin et al. (2000), where
474 there is a wide more dilute finer grain top layer and a channelized sediment-rich layer on the
475 bottom. The two layer model can apply to TRAN because the lahar at this monitoring station
476 overtook the channel (Figure 2d,e) and proceeded to flow horizontally outward forming the
477 surface layer described by Cronin et al. (2000).

478 **4.3 Implications for monitoring**

479 The main goal of this research is to contribute in defining better monitoring criteria for
480 dangerous mass flow events. The data described above is part of a larger collection of
481 monitoring data collected over the entire length of the Whangaehu channel consisting of 21
482 monitoring sites and years of preparation (e.g. Manville and Cronin, 2007; Keys and Green,

Deleted: 7

Deleted: 2

2008). Due to this, the ability to accurately estimate the properties of the lahar at various stages along its path is possible. When it comes to flow events of any size, the ability to understand how the dynamics change with distance along the channel is important for warning and future hazard mitigation. We show here that a lake-breakout event can start out as an outburst flood, bulk up into a hyperconcentrated flow, then eventually elongate and entrap enough sediment to transform into a plug-like slurry flow. Each of these flow types yields differing PSF ranges and patterns due to the relationship between the channel geometry, sediment concentration, turbulence, and bedload transport. While the lahar at different stations along the channel may have differing PSF content, we also show that the lahar elongates and a predictable model (e.g. Cronin et al., 1999) can be used with and shown in the seismic data. Being able to apply such a model may yield some relevance of universality in terms of warning systems at different distances away from the mass flow source. Whereas shown above, the flow phases at each monitoring station can be seen, but at differing lengths and times in the seismic signal (e.g. Figure 6). To better visualize this concept, conceptual models based off of the Cronin et al., 1999 models are created for each of the three seismic stations for the 18 March 2007 lahar (Figure 9). In the conceptual models for the 2007 lahar, the aforementioned elongation of the frontal pulse or bow wave (phase 1) and head of the lahar (phase 2) is shown, along with the differences and similarities between the properties of the lahar at the three seismic monitoring sites.

Deleted: s

Deleted:

Deleted: 8

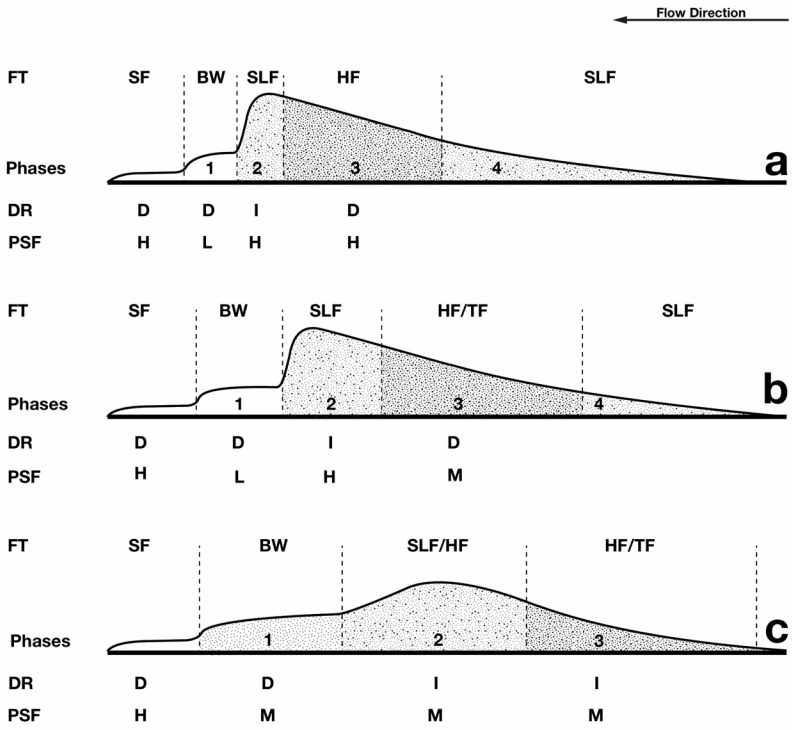

507

508 *Figure 9 Conceptual models for the 18 March 2007 lahar at each of the three monitoring stations along the*
509 *Whangaehu channel depicting flow type and the estimated seismic properties at each flow phase. a) RTMT 7.4 km*
510 *from source, b) TRAN 28 km from source, and c) COLL 83 km from source. Flow types (FT) are as followed;*
511 *streamflow (SF), bow wave streamflow (BW), hyperconcentrated flow (HF), Transitional flow (TF), and sediment-*
512 *laden streamflow (SLF). Note, decreased (D), increased (I), high (H), low (L), and mixed (M) are notations for*
513 *directionality ratios and peak spectral frequency estimates.*

Deleted: *8*

514 Another implication for future warning is the implementation of 3-component sensors and the
515 use of DRs for channels that have streamflow. Walsh et al. (2020) showed for lahars flowing in
516 La Lumbre channel at Volcán de Colima that the DR for streamflow is <1 and then increases
517 when the lahar arrives. This same feature can be seen at each of the three monitoring sites for

519 the 18 March 2007 event (Figure 6) indicating differing flow types will still show this DR pattern
520 within the same flow and at other channels. To further show this, there were three natural non-
521 lake-breakout eruption-based lahars that occurred in the Whangaehu channel in September
522 2007 (for more details on the lahars see Cole et al., 2009; Kilgour et al., 2010) and recorded on
523 the seismometer at RTMT. The DR for the September events starts with streamflow with a DR <
524 1 and when the first lahar arrives the DR increases to >1 and as the lahar fully passes, the DR
525 decreases to <1 again (Figure 10a). As the second lahar arrives at RTMT (Figure 10, second
526 dashed line), the DR increases to >1 again. After the second lahar passes the DR deceases once
527 again back below DR<1. Finally, as the third lahar arrives (Figure 10, third dashed line) the DR
528 yet again increases above 1 for the entirety of the event.

529 For many mass flows and especially those that flow into channels with preexisting streamflow,
530 the peak seismic amplitude does not always coincide with the arrival of the mass flow, and thus
531 may not be the most reliable for event detection or warning. These observations may be due to
532 a frontal surge, the lag in sediment concentration or differences in peak amplitude with peak
533 discharge. Phase 1 (frontal streamflow surge) of the model proposed by Cronin et al. (1999) was
534 based on a hyperconcentrated flow interacting with streamflow, but has also been shown for
535 debris flows as well (e.g. Arratano and Moia, 1999). Arratano and Moia (1999) showed at
536 Moscardo Torrent, Italy, through a hydrograph that there was a precursory surge ahead of the
537 debris flow that was not seen in the seismic record. Similarly, at Ruapehu, for the 18 March
538 2007 lahar, at each of the three stations there is little evidence in the seismic amplitude that
539 there was a precursory surge or phase 1 (Figures 3-5, bottom panel). Conversely, the surge
540 ahead of the lahar can be seen in both the PSF analysis (drop to low frequencies) and in the DR

Deleted: 9

Deleted: 9

Deleted: 9

(decrease in DR) right before the peak seismic amplitude arrives. This shows that when monitoring for future events that not only the amplitude should be used, but other analysis (e.g. PSF, DR) as well, otherwise there could be a delay in the detection of an event.

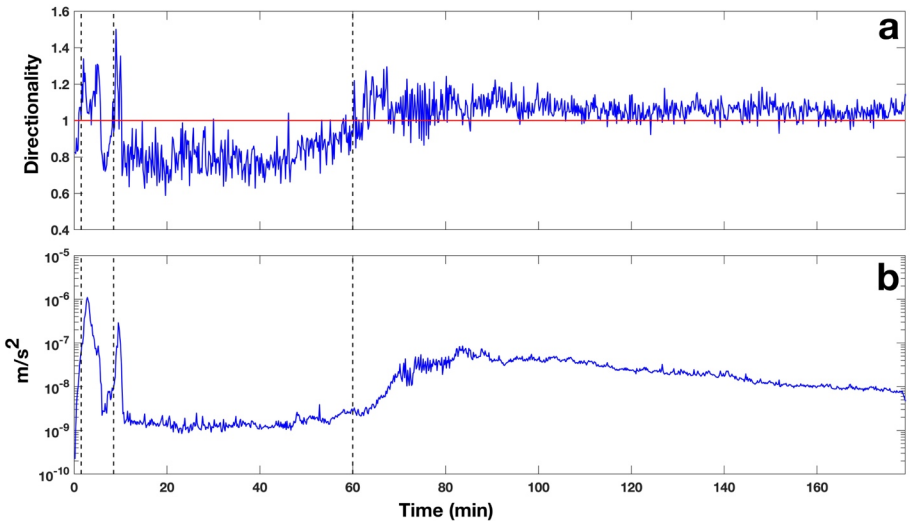

Figure 10 (a) Directionality ratio for the time sequence of the three lahars that occurred on 25 September 2007. (b) RMS amplitude of the seismic record at RTMT during the timing of the three September lahars. Note that the black dashed lines represent the timing of each lahar arriving at the monitoring site.

Deleted: 9

Using all three components of the seismometer can be very beneficial in lahar monitoring. The above-mentioned DR analysis can only be completed with horizontal recording, and analyzing PSF in each component can yield critical information about the flow properties and dynamics. Examining the seismic amplitude differences can generate significant discoveries, for example, when the vertical component is stronger than the horizontal components, bedload dominates over turbulence noise (Burtin et al., 2010). Greater flow parallel signals may indicate higher water transport noises (Barrier et al., 2015) and higher cross-channel signals could be caused by

559 increased interflow particle collisions and flow-channel wall interactions (Doyle et al., 2010).
560 While using the differences in each component can be useful, there are also some concerns.
561 Channel geometry and bed conditions can alter the seismic signal (e.g. Coviello et al., 2019;
562 Marchetti et al., 2019). Additionally, the flow parallel direction can be influenced by the lahar
563 that has already passed, the lahar at the station and the lahar arriving. Furthermore, the tilt of
564 the seismometer may play a large role in determining which component is larger (e.g. Anthony
565 et al., 2018). In the case of the 18 March 2007 lahar a large pulse of water passed the stations
566 which may explain why the parallel component is stronger than the other two components at
567 RTMT and TRAN. At COLL, the lahar had elongated, lost energy, and thus shows more
568 decreased flow parallel energy compared to the previous two stations. In the cross-channel
569 direction, if a flow overtops the channel, the amplitude would presumably be dampened. This
570 may be the case at TRAN where both the flow parallel and vertical directions are more
571 energetic than the cross-channel amplitude after the passing of the head and breaking out of
572 the channel occurred (Figures 2d, 4 bottom row). Another concern when using the horizontal
573 components of a seismometer are the effects shallow layers may have on the site response of
574 the sensor. This is especially true when a sensor is installed on soft or lose sediment (e.g. soil,
575 fluvial/alluvial deposits). To test for potential effects by shallow layer fundamental frequencies,
576 H/V analysis of ambient noise (streamflow dominant) was conducted (see Supplementary
577 material). For RTMT, the H/V results depict a broad frequency peak between 5-15 Hz with a
578 local maximum at ~8 Hz (Figure S4a). Comparing the H/V frequency with the PSF of RTMT
579 (Figure 3), the only overlap is immediately before the front of the lahar passes the station
580 where the PSF decreases for ~1 minute before the head of the lahar arrives. The H/V analysis

for TRAN has a multi- broad-peak shape, with frequency peaks at ~14 and ~28-35 Hz (Figure S4b). While these frequencies are similar to PSF values for TRAN (Figure 4), the H/V analysis has no distinguishable fundamental frequency, contains large error, and no frequency peak has a H/V amplification > 2. In order for a H/V frequency peak to be considered ideal, generally the amplification must to be greater than 2 and the standard deviation lower than a factor of 2 (SESAME, 2004). The H/V amplification for COLL displays a broad frequency peak between 13-18 Hz, with a local maximum at ~18 Hz (Figure S4c). Comparing the PSFs at COLL (Figure 5), only the cross-channel direction has significant PSF values in the same frequency range (~18 Hz band). With all three stations not yielding distinct H/V frequency peaks, we surmise that the PSF content for the 18 March 2007 lake-breakout lahar is most likely dominated by the large flow passing by the seismic sensor rather than large site amplification effects from a shallow layer. While this may be the case, there is still the possibility that some of the PSF values could be due to local effects and should not be considered in the lahar analysis, e.g., the low PSFs at RTMT between 15-20 min (Figure 3), at TRAN contributing to some of the "jumping" in PSF content (Figure 4), or in the mostly dominant 15-20 Hz PSF in the cross-channel direction at COLL. Conversely, SCF values at each station do not reside in the broad H/V frequency range at any station (Figure 7), which may further support the hypothesis that almost all of the recorded frequencies are indeed produced by the lahar. With the use of horizontal components becoming common in mass flow monitoring, future 3-component analyses of mass flows should consider estimating H/V ratios or use other site response methods (e.g. spectral ratio analysis) in order to identify whether near-surface structures may affect the recorded flow data. Overall, all these concerns can and should be tested to estimate potential error in 3-component

Deleted: in the future

Deleted: these

methods. Nevertheless, using all three components of the seismometer can enhance the productivity of warning systems, and if possible, should be used instead of single component sensors.

5. Conclusions

At 23:18 UTC on 18 March 2007 Mt. Ruapehu produced the biggest lahar in New Zealand in over 100 years causing 1.3×10^6 m^3 of water to flow out of the Crater Lake and rush down the Whangaehu channel flowing for over 200 km to the Tasman sea. Seismic analysis at three monitoring locations along the channel (7.4, 28, and 83 km) yielded an understanding of how flow type and processes of the lahar evolve with distance. The proximal lahar was a highly turbulent outburst flood, which generated high PSF content in all three components. Further along the channel after the lahar had bulked up and transformed into a multi-phase hyperconcentrated flow, the PSF content was variable and showed changes in the flow regime/phase. Finally, at the most distal monitoring station, the lahar had lost energy and transformed into a slurry-type flow where the PSF content became more bedload-dominant. Additionally, directionality ratios from all three sites along with data from additional lahars yielded strong evidence that DRs can be used for warning systems when there is streamflow present in the channel. Furthermore, PSF and DRs show evidence of a pre-lahar water pulse that is concealed in the raw seismic data, but has been observed visually. Ultimately, the use of 3-component broadband seismic analysis for the 18 March 2007 lahar at Mt. Ruapehu may lead to more accurate and advanced real-time warning systems for mass flows through the use of frequency and directionality around the world.

Deleted: c

Deleted: l

Author Contribution

BW performed seismic analysis and drafted the manuscript, CL organized and prepared data, and JP created the visual location representation of the event. All participating authors contributed to the discussions and editing of the draft of the manuscript, as well as approving the final edition.

Competing Interests

The authors declare that they have no conflict of interest

Acknowledgements

This work was supported by the Resilience to Natures Challenges – New Zealand National Science, volcano program of research. We would also like to thank all the people from Massey University, Horizons Regional Council, NIWA, and the Department of Conservation that collected data and set up monitoring locations all along the channel in preparation for and during the lahar. A final special thanks to Kate Arentsen for editorial support.

References

Anthony, R., Aster, R., Ryan, S., Rathburn, S., Baker, M.: Measuring mountain river discharge using seismographs emplaced within the hyporheic zone, *Journal of Geophysical Research: Earth Surface, 123, 210-228, 2018.*

Arattano, M., Marchi, L.: Measurements of debris flow velocity trough cross-correlation of instrumentation data, *Natural Hazards and Earth System Sciences, 5, 137-142, 2005.*

Deleted: , 2018,

Deleted: v.

Deleted: p.

Deleted: , 2005,

Deleted: v.

Deleted: p.

Arattano, M., Moia, F.: Monitoring the propagation of debris flow along a torrent, *Hydrological Sciences- Journal des Sciences Hydrologiques, 44(5), 811-823, 1999*.

Barriere, J., Oth, A., Hostache, R., Krein, A.: Bed load transport monitoring using seismic observations in a low-gradient rural gravel bed stream, *Geophys. Res. Lett., 42, 2294-2301, 2015*.

Bartholomaus, T., Amundson, J., Walter, J., O'Neel, S., West, M., Larsen, C.: Subglacial discharge at tidewater glaciers revealed by seismic tremor, *Geophys. Res. Lett., 42, 6391-6398, 2015*.

Burtin, A., Vergne, J., Rivera, L., Dubernet, P.: Location of river-induced seismic signal from noise correlation functions, *Geophys. J. Int., 182, 1161-1173, 2010*.

Capra, L., Borselli, L., Barley, N., Ruiz, J., Norini, G., Sarocchi, D., Caballero, L., Cortes, A.: Rainfall-triggered lahars at Volcan de Colima, Mexico: Surface hydro-repellency as initiation process, *Journal of Volcanology and Geothermal Research, 198, 105-117, 2010*.

Capra, L., Coviello, V., Borselli, L., Marquez-Ramirez, V., Arambula-Mendoza, R.: Hydrological control of large hurricane-induced lahars: evidence from rainfall-runoff modeling, seismic and video monitoring, *Nat. Hazards Earth Syst. Sci., 18, 781-794, 2018*.

Carrivick, J., Manville, V.: A fluid dynamics approach to modelling the 18th March 2007 lahar at Mt. Ruapehu, New Zealand, *Bull. Volcanol., 71, 153-169, 2009*.

Cole, S., Cronin, S., Sherburn, S., Manville, V.: Seismic signals of snow-slurry lahars in motion: 25 September 2007, Mt Ruapehu, New Zealand, *Geophys. Res. Lett., 36, L09405, 2009*.

Deleted: , 1999,
Deleted: v.
Deleted: , p.
Deleted: , 2015,
Deleted: v.
Deleted: p.
Deleted: , 2015,
Deleted: v.
Deleted: p.
Deleted: , 2010,
Deleted: v.
Deleted: p.
Deleted: , 2010,
Deleted: v.
Deleted: p.
Deleted: , 2018,
Deleted: v.
Deleted: p.
Deleted: , 2009,
Deleted: v.
Deleted: p.
Deleted: , 2009,

Coviello, V., Arattano, M., Comiti, F., Macconi, P., Marchi, L.: Seismic characterization of debris flows: Insights into energy radiation and implications for warning, *Journal of Geophysical Research: Earth Surface, 124, 2019*.

Coviello, V., Capra, L., Vazquez, R., Marquez-Ramirez, V.: Seismic characterization of hyperconcentrated flows in a volcanic environment, *Earth Surf. Process. Landforms., 43, 2219-2231, 2018*.

Cronin, S., Neall, V., Jerome, L., Palmer, A.: Unusual "snow slurry" lahars from Ruapehu volcano, New Zealand, September 1995, *Geology, 24, 1107-1110, 1996*.

Cronin, S., Neall, V., Jerome, L., Palmer, A.: Dynamic interactions between lahars and stream flow: A case study from Ruapehu volcano, New Zealand, *GSA Bulletin, 111(1), 28-38, 1999*.

Cronin, S., Neall, V., Jerome, L., Palmer, A.: Transformation, internal stratification, and depositional processes within a channelized, multi-peaked lahar flow, *New Zealand Journal of Geology and Geophysics, 43, 117-128, 2000*.

Doyle, E., Cronin, S., Cole, S., Thouret, J.: The coalescence and organization of lahars at Semeru volcano, Indonesia, *Bull. Volcanol., 72, 961-970, 2010*.

Doyle, E., Cronin, S., Cole, S., Thouret, J.: Defining conditions for bulking and debulking in lahars, *GSA Bulletin, 123, 1234-1246, 2011*.

Huang, C., Shieh, C., Yin, H.: Laboratory study of the underground sound generated by debris flows, *Journal of Geophysical Research, 109, F01008, 2004*.

Deleted: , 2019,
Deleted: v.
Deleted: , 2018,
Deleted: v.
Deleted: p.
Deleted: , 1996,
Deleted: v.
Deleted: p.
Deleted: , 1999,
Deleted: v.
Deleted: , n.
Deleted: p.
Deleted: , 2000,
Deleted: v.
Deleted: p.
Deleted: , 2010,
Deleted: v.
Deleted: p.
Deleted: , 2011,
Deleted: v.
Deleted: p.
Deleted: , 2004,
Deleted: v.

Iguchi, M.: Proposal of estimation method for debris flow potential considering eruptive activity, *Journal of Disaster Research, 14(1), 126-134, 2019.*

Gimbert, F., Tsai, V., Lamb, M.: A physical model for seismic noise generation by turbulent flow in rivers, *Journal of Geophysical Research: Earth Surface, 119, 2209-2238, 2014.*

Keys, H., Green, P.: Ruapehu lahar New Zealand 18 March 2007: Lessons for hazard assessment and risk mitigation 1995-2007, *Journal of Disaster Research, 3(4), 284-296, 2008.*

Kilgour, G., Manville, V., Della Pasqua, F., Graettinger, A., Hodgson, K., Joly, G.: The 25 September 2007 eruption of Mount Ruapehu, New Zealand: Directed ballistics, surtseyan jets, and ice-slurry lahars, *Journal of Volcanology and Geothermal Research, 191, 1-14, 2010.*

Kogelnig, A., Surinach, E., Vilajosana, I., Hubl, J., Sovilla, B., Hiller, M., Dufour, F.: On the complementariness of infrasound and seismic sensors for monitoring snow avalanches, *Nat. Hazards Earth Syst. Sci., 11, 2355-2370, 2011.*

Kuehnert, J., Mangeney, A., Capdeville, Y., Vilotte, J., Stutzmann, E., Chaljub, E., et al.: Locating rockfalls using inter-station ratios of seismic energy at Dolomieu crater, Piton de la Fournaise volcano, *Journal of Geophysical Research: Earth Surface, 126, e2020JF005715, 2021.*

Lube, G., Cronin, S., Manville, V., Procter, J., Cole, S., Freundt, A.: *Geology, 40, 475-478, 2012.*

Manville, V., Cronin, S.: Breakout lahar from New Zealand's crater lake, *EOS Transactions, 88(43), 441-456, 2007.*

Deleted: , 2019,

Deleted: *v.*

Deleted: *p.*

Deleted: ., 2014,

Deleted: *v.*

Deleted: *p.*

Deleted: , 2008,

Deleted: *v.*

Deleted: *, n.*

Deleted: *p.*

Deleted: , 2010,

Deleted: *v.*

Deleted: *p.*

Deleted: , 2011,

Deleted: *v.*

Deleted: *p.*

Deleted: , 2021

Deleted: ,

Deleted: , 2012,

Deleted: *v.*

Deleted: *p.*

Deleted: , 2007,

Deleted: *v.*

Deleted: *, n.*

Deleted: *p.*

Manville, V., White, J., Hodgson, K.: Dynamic interactions between lahars and stream flow: A case study from Ruapehu volcano, New Zealand: Discussion and reply discussion, *GSA Bulletin, 112(7), 1149-1152, 2000.*

Marchetti, E., Walter, F., Barfucci, G., Genco, R., Wenner, M., Ripepe, M., McArdell, B., Price, C.: Infrasound array analysis of debris flow activity and implications for early warning, *Journal of Geophysical Research: Earth Surface, 124, 567-587, 2019.*

Massey., C., Manville, V., Hancox, G., Keys, H., Lawrence, C., McSaveney, M.: Out-burst flood (lahar) triggered by retrogressive landsliding, 18 March 2007 at Mt Ruapehu, New Zealand – a successful early warning, *Landslides, 7, 303-315, 2010.*

O'Connor, J., Clague, J., Walder, J., Manville, V., Beebee, R.: Outburst Floods, *Reference Module in Earth Systems and Environmental Sciences, Elsevier, 2020.*

O'Shea, B.: Ruapehu and the Tangiwai disaster, *NZ J. Sci. Tech. 36B, 174-189, 1954.*

Pardo, N., Cronin, S., Palmer, A., Nemeth, K.: Reconstructing the largest explosive eruptions of Mt. Ruapehu, New Zealand: Lithostratigraphic tools to understand subplinian-plinian eruptions at andesitic volcanoes, *Bull. Volcanol., 74, 617-640, 2012.*

Pierson, T., Janda, R., Thouret, J., Borrero, C.: Perturbation and melting of snow and ice by the 13 November 1985 eruption of Nevado del Ruiz, Colombia, and consequent mobilization, flow and deposition of lahars, *J. Volcanol. Geotherm. Res., 41(1), 17-66, 1990.*

Pierson, T., Scott, K.: Downstream dilution of a lahar: Transition from debris flow to hyperconcentrated streamflow, *Water Resources Research, 21(10), 1511-1524, 1985.*

Deleted: , 2000,
Deleted: v.
Deleted: , n.
Deleted: p.
Deleted: , 2019,
Deleted: v.
Deleted: p.
Deleted: , 2010,
Deleted: v.
Deleted: p.
Deleted: ,
Deleted: 2020,
Deleted: , 1954,
Deleted: , 2012,
Deleted: v.
Deleted: p.
Deleted: , 1990,
Deleted: v.
Deleted: p.
Deleted: , 1985,
Deleted: v.
Deleted: , n.
Deleted: p.

Procter, J., Cronin, S., Fuller, I., Lube, G., Manville, V.: Quantifying the geomorphic impacts of a lake-breakout lahar, Mount Ruapehu, New Zealand, *Geology, 38, 67-70, 2010*.

Procter, J., Cronin, S., Sheridan, M.: Evaluation of Titan2D modelling forecasts for the 2007 Crater Lake break-out lahar, Mt. Ruapehu, New Zealand, *Geomorphology, 136, 95-105, 2012*.

Procter, J., Cronin, S., Fuller, I., Sheridan, M., Neall, V., Keys, H.: Lahar hazard assessment using Titan2D for an alluvial fan with rapidly changing geomorphology: Whangaehu River, Mt. Ruapehu, *Geomorphology, 116, 162-174, 2010*.

Procter, J. N., Cronin, S. J., Zernack, A. V., Lube, G., Stewart, R. B., Nemeth, K., & Keys, H.: Debris flow evolution and the activation of an explosive hydrothermal system; Te Maari, Tongariro, New Zealand. *Journal of Volcanology and Geothermal Research*, *286*, 303-316, 2014.

Procter, J., Zernack, A., Mead, S., Morgan, M., & Cronin, S.: A review of lahars; past deposits, historic events and present-day simulations from Mt. Ruapehu and Mt. Taranaki, New Zealand. *New Zealand Journal of Geology and Geophysics*, *64*(2-3), 479-503, 2021.

Roth, D., Brodsky, E., Finnegan, N., Rickenmann, D., Turowski, J., Badoux, A.: Bed load sediment transport inferred from seismic signals near a river, *J. Geophys. Res. Earth Surf., 121, 725-747, 2016*.

Schimmel, A., Coviello, V., Comiti, F.: Debris-flow velocity and volume estimations based on seismic data, *Natural Hazards and Earth System Sciences, 2021*.

Deleted: , 2010,

Deleted: *v.*

Deleted: *p.*

Deleted: , 2012,

Deleted: *v.*

Deleted: *p.*

Deleted: , 2010,

Deleted: *v.*

Deleted: *p.*

Deleted: (2014).

Deleted: (2021).

Deleted: , 2016,

Deleted: b

Deleted: *P.*

Deleted: , 2021,

Schmandt, B., Aster, R., Scherler, D., Tsai, V., Karlstrom, K.: Multiple fluvial processes detected by river side seismic and infrasound monitoring of a controlled floor in the Grand Canyon, *Geophys. Res. Lett.*, *40(18)*, *4858-4863*, *2013*.

Schmandt, B., Gaeuman, D., Stewart, R., Hansen, S., Tsai, V., Smith, J.: Seismic array constraints on reach-scale bedload transport, *Geology*, *45*, *299-302*, *2017*.

Saló, L., Corminas, J., Lantada, N., Mata, G., Prades, A., Ruiz-Carulla, R.: Seismic energy analysis as generated by impact and fragmentation of single-block experimental rockfalls, *Journal of Geophysical Research: Earth Surface, 123, 1450-1478, 2018.*

Scott, K.: Origins, behavior, and sedimentology of lahars and lahar runout flows in the Toutle-Cowlitz river system, *USGS Professional Paper*, *1988*.

Surinach, E., Vilajosana, I., Khazaradze, G., Biescas, B., Furdada, G., Vilaplana, J.: Seismic detection and characterization of landslides and other mass movements, *Natural Hazards and Earth System Sciences*, *5*, *791-798*, *2005*.

Walsh, B., Coviello, V., Capra, L., Procter, J., Marquez-Ramirez, V.: Insights into the internal dynamics of natural lahars from analysis of 3-component broadband seismic signals at Volcán de Colima, Mexico, *Front. Earth Sci. 8*, *542116*, *2020*.

Walsh, B., Jolly, A., Procter, J.: Seismic analysis of the 13 October 2012 Te Maari, New Zealand, lake breakout lahar: Insights into flow dynamics and the implications on mass flow monitoring, *J. Volcanol. Geotherm. Res.*, *324*, *144-155*, *2016*.

Deleted: , 201
Deleted: 3,
Deleted: *v.*
Deleted: *p.*
Deleted: , 2017,
Deleted: *v.*
Deleted: *p.*
Formatted: Font: Italic
Deleted: , 1988,
Deleted: , 2005,
Deleted: *v.*
Deleted: *p.*
Deleted: , 2020,
Deleted: :
Deleted: , 2016,
Deleted: *v.*
Deleted: *p.*